DOI: 10.1002/fuce.200800049

Fuel Cells

ORIGINAL RESEARCH PAPER

Analysis of the Ripple Current in a 5 kW Polymer Electrolyte Membrane Fuel Cell Stack

B. P. Ladewig[1]*, and F. Lapicque[1]

[1] Laboratoire des Sciences du Génie Chimique, CNRS-ENSIC, 1 rue Grandville, BP 20451, 54001 Nancy Cedex, France

Received July 04, 2008; accepted December 27, 2008

Abstract

Polymer electrolyte fuel cell systems are increasingly being used in applications requiring an inverter to convert the direct current (DC) output of the stack to an alternating current (AC). These inverters, and other time-varying inputs to the stack such as the anode feed pressure, cause deviations from the average stack current, or ripple currents, which are undesirable for reasons of performance and durability. A dynamic fuel cell model has been developed and validated against experimental data for a 5 kW fuel cell stack, examining in detail the ripple current behaviour. It was shown that the ripple currents exceed the 2% maximum recommended value, and may lead to long-term degradation of the fuel cell stack.

Keywords: Combined Heat and Power, Dynamic Model, Fuel Cell Model, PEM Fuel Cell, Ripple Current

1 Introduction

Proton exchange membrane (PEM) fuel cells have recently been considered for use as stationary power sources for residential and commercial buildings because of their potential to provide a clean, quiet, scalable and reliable supply of electricity, whilst also producing heat that may be recovered [1–5]. They are also being developed as uninterrupted power supply (UPS) systems for applications including mobile phone base stations [6]. In these applications, the direct current (DC) output of the fuel cell stack, which ranges from 24–150 V_{DC} depending on the number of cells, must be converted to an alternating current (AC) to interface with the relevant utilities [7]. This is usually accomplished using a DC–DC converter to boost the voltage to a useful level and an inverter to produce an AC. For residential applications a single- or dual-phase inverter may be used, while for industrial applications a three-phase inverter is more suitable.

Although, there are various power conditioning topologies available for conditioning a fuel cell DC current [7], one of the key difficulties faced by fuel cell designers is the introduction of ripple currents by the inverter. Ripple currents is the term given to deviations from the average fuel cell current, although more precise definitions such as the deviation from the instantaneous fuel cell theoretical current [8] have been proposed. Ripple currents can have an adverse impact on fuel cell durability because of degradation of the membrane electrode assembly [9], due to the local depletion of hydrogen at the anode catalyst. Ripple currents can also contribute to unnecessary system downtime when the peak current (i.e. the average current plus the peak current) exceeds the maximum safe operating current and causes the system to ramp or shut down. It is now known from extensive field trial experience that disruptions such as this cause a significant reduction in the fuel cell stack lifetime [10], and should be avoided where possible.

In this work, we have developed a dynamic mathematical model of a 5 kW fuel cell stack and validated it using experimental data. To examine in detail the ripple current behaviour, we have perturbed the model using time-varying inputs of anode feed pressure and external system resistance obtained from experimental measurements.

2 Fuel Cell System

2.1 Fuel Cell Experimental System

The fuel cell stack was supplied by Hélion Fuel Cell company and contained 75 cells of 342 cm^2 active area. It was

[*] *Corresponding author, bradley.ladewig@eng.monash.edu.au*

installed in a combined heat and power system using a natural gas reformer and hydrogen purification membrane unit from Idatech LLC, similar to that described by Löffler et al. [11]. The DC output from the fuel cell stack was inverted to 240 V AC using an inverter supplied by Sustainable Energy Technologies Ltd [12]. The system was installed at the FC-Lab in Belfort, France and fed with natural gas from the local reticulated supply.

2.2 Fuel Cell Model

The modelling approach and basic stack model are based on that of Khan and Iqbal [13], with modifications and additions detailed explicitly as follows.

The output voltage of a single cell, V_{cell} is expressed as the sum of three components: the Nernst potential, E_{Nernst}, the activation overpotential η_{act} and the ohmic overpotential η_{ohm}.

$$V_{cell} = E_{Nernst} - \eta_{act} - \eta_{ohm} \quad (1)$$

The activation potential covers the irreversibility at the two electrodes. A concentration overpotential term was not included in this model, because Eq. (1) was capable of describing the potential drop at high current density with appropriate parametric modelling [14–16]. Furthermore, the operating current density of the experimental system did not extend into the region of the polarisation curve characteristic of mass transfer limitation.

The total stack voltage, V_{stack}, is then the product of the individual cell voltage and the number of cells, N.

$$V_{stack} = NV_{cell} \quad (2)$$

The temperature-dependent form of the Nernst equation gives the Nernst potential as a function of the hydrogen and oxygen partial pressures, p'_{H_2} and p'_{O_2} (atm) respectively, and the temperature, T (K). R is the universal gas constant, F Faraday's constant and $E°$ is the standard cell potential (1.229 V).

$$E_{Nernst} = E° - 8.5\times10^{-4}(T - 298.15) + RT/2F \ln\left[p'_{H_2}\sqrt{p'_{O_2}}\right] \quad (3)$$

2.3 Expressions for the Various Overpotentials

The model developed by Khan and Iqbal concerned the use of Nafion membranes coated with platinum-based electrodes. In the present study, the membranes were 18 μm thick fluorosulfonate polymer sheets and the electrodes had been prepared with 40 wt% Pt suspension, resulting in 0.4 mg Pt cm^{-2} on the carbon-based support. Because the overall conductivity of the coated membrane depends on the procedure applied for MEA assembly, it was preferred to measure the overall ohmic resistance of the MEA. In addition, the activity of the electrodes considered here may differ from those used in the previous works of Amphlett's group [14–16].

2.3.1 Determination at Fixed Pressures of the Reacting Gases

Similar MEAs were tested at bench scale, with 25 cm^2 single cells operated at 70 °C; the other operating conditions were kept as close as possible as those in the large stack. Hydrogen and air were continuously fed at 1.6 bars with stoichiometric factors of 1.2 and 2.0, respectively. Only air was humidified at 70%. The flow field in the small single cell differed from that in the larger cells because of the very different plate dimensions. Nevertheless, the flow fields in the two systems were of comparable design.

For fixed values of the current density, the cell voltage was monitored for 1 h or more; impedance spectra were thereafter recorded for frequency ranging from 20 kHz to 0.1 Hz. Voltage *versus* current density variations in the small cell were shown to be in good agreement with the cell performance of the large stack [17].

Spectra in Nyquist plot consisted of two loops: the first one at high/middle-range frequencies corresponding to charge transfer at the electrodes, the second one below 1 Hz expressing possible mass transfer control at the cathode. Impedance spectra were interpreted considering a simple equivalent circuit, neglecting in this approach the contribution of the anode. As described in reference papers [18, 19], the circuit consisted of the ohmic resistance, r_{ohm}, in series with a constant phase element (CPE, with parameter Q and n) in parallel with the activation resistance, r_{act}, and the Warburg element for mass transfer control with resistance r_d and characteristic time t_d. Estimation of the circuit parameters was carried out by minimising the sum of squared residues between the experimental and theoretical components of both real and imaginary parts of the impedance. Because of the numerous parameters involved the fitting was conducted in two steps as follows: (i) the high/middle-range frequency part of the spectra was treated with postulated values for the parameters involved in the low frequency loop; (ii) the obtained values for parameters r_{ohm}, r_{act}, Q and n were used for the fitting of the low-frequency part of spectra, yielding improved values for diffusion resistance. As a matter of fact, exponent n of the CPE was found in most of the cases to be more than 0.95, allowing the CPE to be approximated by a pure capacitor, with capacitance C_{dl}.

The membrane resistance r_{mem} was approximated by r_{ohm}, neglecting for single cell investigations the contributions of metal plates and the current leads in the overall resistance. The equivalent electrical conductivity of the MEA was obtained taking into account the membrane thickness, l_{mem}, and its area, A.

$$r_{mem} = \frac{l_{mem}}{\sigma_{mem}A} \quad (4)$$

The following polynomial function was fitted to the experimental data:

$$\frac{1}{\sigma_{mem}} = 0.0298\left(\frac{i}{A}\right)^2 - 0.0688\left(\frac{i}{A}\right) + 0.177 \quad (5)$$

Electrical resistance is also present in the bipolar plates and the wires connecting the fuel cell stack to the inverter. This was accounted for in the stack model using a constant value of 0.5 mΩ, which was obtained by fitting the model to experimental results.

The current density was expressed as a function of the electrode overvoltage η depending on exchange current density, i_0, Tafel slope, b, and limiting current density i_L as follows:

$$i = \frac{2i_0 \sinh(b\eta)}{\frac{1+2i_0}{i_L}\sinh(b\eta)} \tag{6}$$

The activation resistance can be defined as the partial derivative function of the limiting current density with respect to overpotential η, at fixed values of concentrations

$$r_{act} = \frac{\partial\eta}{\partial i} = \frac{1}{\partial i / \partial\eta} = \frac{[i_L + 2i_0\sinh(b\eta)^2}{2i_L^2 i_0 b\cosh(b\eta)} \tag{7}$$

Theoretical variations of the activation resistance with overpotential were calculated as follows. For postulated values of parameters i_0, b and i_L: a value for η was chosen, the corresponding values for i and r_{act} were simply calculated using the above two relations. Fitting the theoretical variation to the experimental data in the form of (R_{act}, i) couple led to the parameter values:

$i_0 = 7 \times 10^{-6}$ A cm^{-2}, $b = 26.35$ V^{-1} and $i_L = 1.35$ A cm^{-2}

Moreover the variation of the cell voltage with the current density could be predicted from the kinetic law (6) and the value for the membrane resistance (5): the experimental variation was found to be in good agreement with the predicted variation. It has to be mentioned that in the experimental current density range the contribution of mass transfer rate expressed by i_L was of little significance.

2.3.2 *Kinetic Law for Varying Pressures of Reacting Gases*

The fluctuations of hydrogen and oxygen pressures induced by the operation of the fuel cell induced periodic variations of the activation overpotential. Such fluctuations cannot be accounted for by Eq. (6). It was thereafter decided to adapt the relation employed by Khan and Iqbal to the present case:

$$\eta_{act} = \xi_1 + \xi_2 T + \xi_3 T\left[\ln\left(c'_{O_2}\right)\right] + \xi_4 T[\ln(i)] \tag{8}$$

It can be observed that Eq. (8) is a general Tafel law. A generalised steady-state set of expressions for the empirical parameters had been used [13] where c_{H_2} is the concentration of hydrogen at the electrode/membrane interface.

$$\xi_1 = -0.94 \tag{9}$$

$$\xi_2 = 0.00286 + 0.0002\ln(A) + 4.3\times10^{-5}\ln\left(c'_{H_2}\right) \tag{10}$$

$$\xi_3 = 7.6\times10^{-5} \tag{11}$$

$$\xi_4 = -1.93\times10^{-4} \tag{12}$$

For current density far lower than i_L comparison of Eqs. (6) and (8) leads to

$$\xi_4 T = \frac{1}{b} \tag{13}$$

Using the value for parameter b yielded a new value for $\xi_4 = -1.11 \times 10^{-4}$. The solubilities of hydrogen and oxygen in the membrane material used for this fuel cell stack were unavailable, so corresponding data for Nafion® were used [20] along with Henry's Law to determine the concentration of oxygen and hydrogen at the electrode/membrane interfaces. It was assumed that since both Nafion and the membrane used in this work are chemically similar the gas solubilities will be similar.

$$c'_{O_2} = \frac{p'_{O_2}}{1.97\times10^7\exp\left(\frac{498}{T}\right)} \tag{14}$$

$$c'_{H_2} = \frac{p'_{H_2}}{0.255\times10^5\exp\left(\frac{170}{T}\right)} \tag{15}$$

Table 1 Fuel cell model parameters.

Symbol	Parameter	Value	Units	Reference
N	Number of cells	75		
F	Faraday's constant	96 485.3	C mol^{-1}	
A	Cell area	342	cm^2	[21]
l	Polymer electrolyte membrane thickness	0.020	mm	[21]
$E°$	Standard cell potential (25 °C)	1.229	V	[23]
R	Ideal gas constant	8.314	J mol^{-1} K^{-1}	
C_{dl}	Double layer capacitance	8.69	F	[21]
Vol_{ca}	Cathode compartment volume	0.01	m^3	[13], assumed
k_{ca}	Cathode outlet flow constant	0.065	mol s^{-1} bar^{-1}	[13], assumed
P_{BPR}	Regulated cathode back pressure	1.3	bar	assumed

Equations (8–11) and (13–15) were applied with hydrogen and air pressures at 1.6 bar: the obtained variation of the activation potential was compared to those calculated using Eq. (6). Figure 1 shows that the expressions used in Reference [13] with the modified values for parameter ξ_4 allow excellent prediction of the activation overpotential for current densities below 0.5 A cm^{-2}.

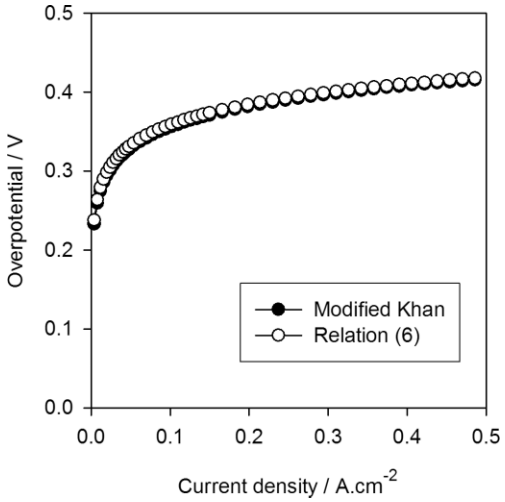

Fig. 1 Comparison between modified Khan expression for the activation overpotential and relation (6).

2.4. Development of the Model with Gas Fluctuations

The recorded profiles of hydrogen pressures can be used straightforward in Eqs. (3) and (10). The oxygen partial pressure is proportional to the quantity of oxygen inside the cathode compartment. This quantity may be calculated using the flows into and out of the stack and the quantity electrochemically consumed, where Vol_{ca} is the cathode volume.

$$\frac{Vol_{ca}}{RT}\frac{d\left(p'_{O_2}\right)}{dt} = \dot{m}_{O_2,in} - \dot{m}_{O_2,out} - \frac{Ni}{4F} \tag{16}$$

The cathode is maintained at a pressure above ambient using a backpressure regulator, and hence the flow out of the cathode is proportional to the difference between the cathode pressure and the regulated backpressure.

$$\dot{m}_{O_2,out} = k_{ca}\left(p_{O_2} - p_{BPR}\right) \tag{17}$$

Due to the development of an electrical double layer at the membrane electrode interfaces, the stack voltage does not respond instantaneously to a change in stack current, instead exhibiting a delay. The overall current i is the sum of the capacitive component and the faradaic contribution. This response may be modelled as a first-order differential system resulting from the expression of the global current, being the sum of the capacitive component and the faradaic component. V_{act} is the voltage drop due to the activation overpotential, r_{act} is the activation resistance and C_{dl} the double layer capacitance of a single cell, which was 8.69 F in this work [21]. This value is consistent with the capacitance determined from single cell experiments, of approximately 0.02 F per geometrical square centimetre.

$$V_{act} = -\eta_{act} \tag{18}$$

$$r_{act} = \frac{\partial V_{act}}{\partial i} \approx \frac{V_{act}}{i} \tag{19}$$

$$\frac{dV_{act}}{dt} = \frac{1}{C_{dl}} - \frac{V_{act}}{r_{act}C_{dl}} \tag{20}$$

The ohmic overpotential results from resistive losses in the stack and electrical connections. Within the stack, a major component of the overall resistance arises from the PEM's resistance to proton flow. The ohmic overpotential is the product of the current and the internal resistance, r_{int}.

$$\eta_{ohmic} = -ir_{int} \tag{21}$$

where the internal resistance r_{int} is the sum of the membrane resistance and the contribution from bipolar plates and the connection wires mentioned above.

2.5 Model Implementation

The model was implemented in MATLAB/Simulink® and solved using the *ode23tb (stiff/TR-BDF2)* solver. A number of parameters were included from experimental runs, as described below.

2.5.1 Anode Hydrogen Feed Pressure

The stack anode was operated in a dead-end configuration, which leads to high hydrogen utilisation at the expense

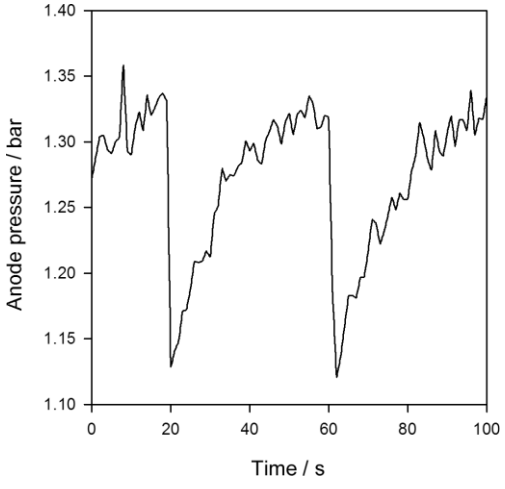

Fig. 2 Typical anode feed pressure fluctuations.

of a somewhat uneven current distribution and the accumulation of water droplets at the end of the flow field. To remove the water droplets, the anode was periodically purged. This leads to a rapid drop in the anode partial pressure of hydrogen (which is measured at the inlet to the stack anode), which then gradually builds up after the purge valve is closed, as shown in Figure 2. For the fuel cell model to accurately reflect the operation of the stack, the anode inlet pressure (as measured during experiments) was recorded and provided as an input to the model.

2.5.2 External Electrical Resistance

A key focus of this work was the impact that variations in the external resistance (due to rapid fluctuations in the internal resistance of the inverter) have on the fuel cell behaviour. Assuming that the resistance of the stack and the electrical connections are approximately constant (when the stack operates at constant temperature), then the fluctuations in the resistance of the inverter may be calculated from the measured system current and voltage output.

$$R_{\text{inv}} = \frac{V_{\text{sys}}}{i} \tag{22}$$

These resistance variations, as shown in Figure 3, were provided to the model as inputs.

3 Results and Discussion

Figure 4 shows the experimental and modelled stack voltage over a period of 100 s (the simulation was run for 600 s with similar results; however for reasons of clarity only 100 s is shown). The simulated result very closely follows the experimental value, within a tolerance of 1 V, which is equivalent to a relative error of less than 2%. It is interesting to note that the model generally shows less variation than the experimental result, i.e. it underestimates the highest voltages and overestimates the lowest voltages, indicating that the model still requires further refinement. Figure 5 shows the corresponding experimental and modelled stack currents, with very good agreement between the two. The modelled result does not deviate from the experimental value by more than 1 A, equivalent to a relative error less than 1%.

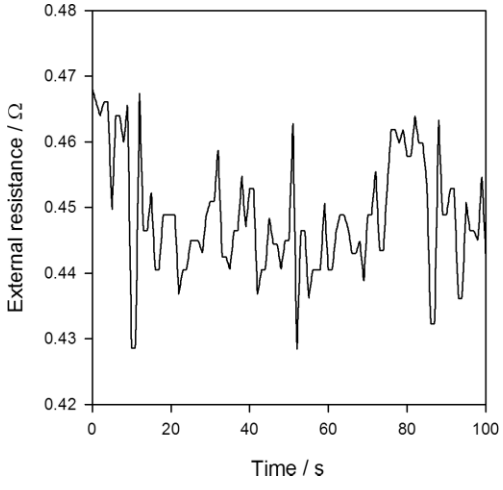

Fig. 3 Typical fluctuations in the external resistance.

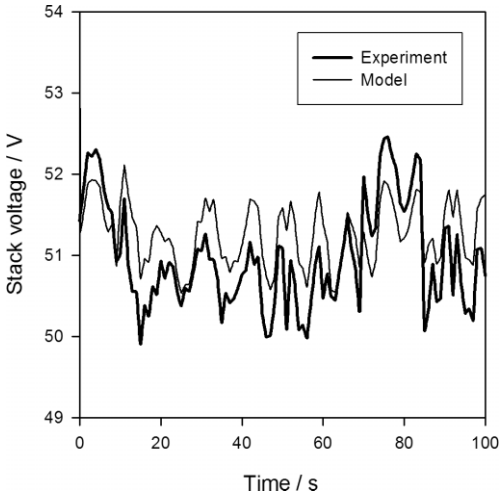

Fig. 4 Experimental (thick line) and modelled (thin line) stack voltage.

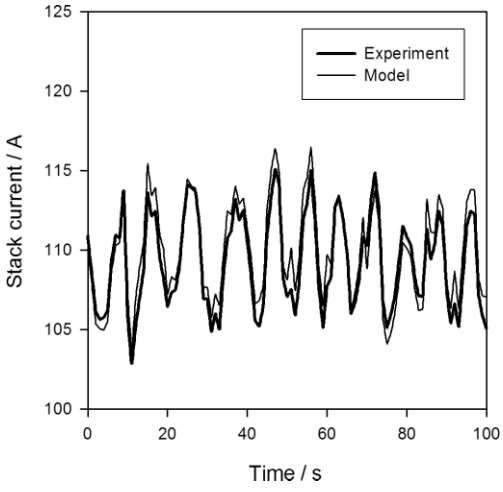

Fig. 5 Experimental (thick line) and modelled (thin line) stack current.

Of some concern is the magnitude of the fluctuations in the stack current. Over the 100 s time period shown in Figure 5, the average current is 109.31 A; however the upper and lower peak currents are 115.07 and 102.85 A, respectively. It has been suggested that ripple currents should not exceed 2% of the average current [8], and hence there is a strong possibility that this system will experience long-term degradation due to these ripple currents.

To analyse the periodic nature of the fluctuation in the anode pressure, the estimated power spectrum, P, was calculated using the Fast Fourier Transform (FFT) of the pressure transducer signal over a time period of 600 s.

$$Y = FFT(p'_{H_2}) \quad (23)$$

$$P = |Y|^2 \quad (24)$$

The power spectrum for the disturbances in the external resistance was calculated likewise, and both spectra are plotted against period (1/frequency) in Figures 6 and 7. The experimental data were recorded every second, and hence the spectra do not extend below a period of 2 s (which is the minimum observable period in time series data with a resolution of 1 s). The fluctuations in the anode pressure are as expected; the purge sequence causes a large peak at a period of 42 s. The peak is not perfectly sharp because, as shown in Figure 2, the drop in pressure is very rapid; however the increase back to the steady-state value takes a longer period of time. The smaller peaks at 21, 14, 10 s and lower are harmonics of the original peak.

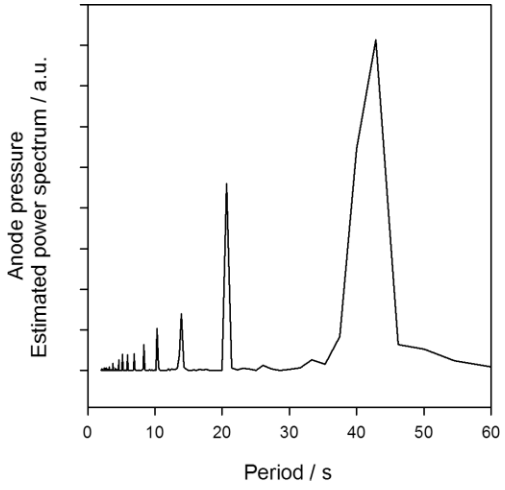

Fig. 6 Anode pressure power spectrum as a function of period.

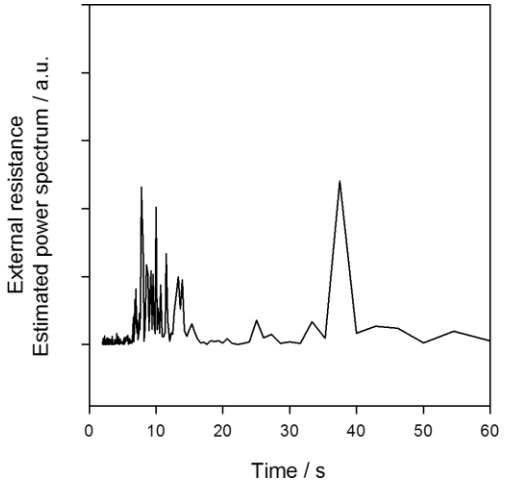

Fig. 7 External resistance power spectrum as a function of time.

The fluctuations in the external resistance show less regular features, with the exception of a large peak around 42 s. This is due to the inverter compensating for the drop of current associated with the purge sequence, and hence is not an independent feature.

A number of methods for limiting the cell ripple current have been proposed [22] and these should be pursued to ensure that the maximum power output and unit lifetime are achieved.

4 Conclusions

A dynamic fuel cell stack model has been developed that is capable of accurately predicting the current and voltage of a 5 kW PEM stack, when provided with the time-varying external resistance and anode feed pressure. The ripple current induced by the inverter has been studied, and shown to exceed recommended safe limits. Further work will examine the effect this ripple current has on long-term durability of the fuel cell stack.

Acknowledgements

The authors thank EDF and ADEME for funding support under the COREPAC program. The technical assistance of Xavier François (UTBM) and Lucile Voiron (Hélion Fuel Cell Company) is gratefully acknowledged.

List of Symbols

C	Capacitance (F)
c	Concentration (mol cm^3)
CPE	Constant phase element
E	Cell potential (V)
$E°$	Standard cell potential (V)
F	Faraday's constant (C mol^{-1})
i	Current (A)
N	Number of cells
p	Partial pressure (atm)
r	Resistance (Ω)
R	Universal gas constant (J mol^{-1} K^{-1})
t	Time (s)
V	Voltage (V)
v	Volume (cm^3)

Greek letters

η	Overpotential
ξ	Empirical coefficient

Subscripts

cell	Single fuel cell
Nernst	Nernst standard cell potential

stack	Fuel cell stack
act	Activation
ohm	Ohmic
H_2	Hydrogen
O_2	Oxygen
dl	Double layer
sys	System
AC	Alternating current
DC	Direct current
ca	Cathode
d	Diffusion

References

[1] P. König, A. Weber, N. Lewald, T. Aicher, L. Jörissen, E. Ivers-Tiffée, *Fuel Cells* **2007**, *7*, 70.

[2] P. König, A. Weber, N. Lewald, T. Aicher, L. Jörissen, E. Ivers-Tiffée, R. Szolak, M. Brendel, J. Kaczerowski, *J. Power Sources* **2005**, *145*, 327.

[3] M. Radulescu, O. Lottin, M. Feidt, C. Lombard, D. L. Noc, S. L. Doze, *J. Power Sources* **2006**, *159*, 1142.

[4] C. Wang, Z. Mao, F. Bao, X. Li, X. Xie, *Int. J. Hydrogen Energy* **2005**, *30*, 1031.

[5] J.-H. Wee, *Renewable and Sustainable Energy Reviews* **2007**, *11*, 1720.

[6] M. Lin, Y. Cheng, M. Lin, S. Yen, *J. Power Sources* **2005**, *140*, 346.

[7] X. Yu, M. R. Starke, L. M. Tolbert, B. Ozpineci, *IET Electric Power Applications* **2007**, *1*, 643.

[8] R. S. Gemmen, *J. Fluid Eng-T. ASME* **2003**, *125*, 576.

[9] W. Shireen, R. A. Kulkarni, A. Arefeen, *J. Power Sources* **2006**, *156*, 448.

[10] B. Du, Q. H. Guo, R. Pollard, D. Rodriguez, C. Smith, J. Elter, *JOM* **2006**, *58*, 45.

[11] D. G. Löffler, K. Taylor, D. Mason, *J. Power Sources* **2003**, *117*, 84.

[12] Sustainable Energy Technologies Ltd, www.sustainableenergy.com

[13] M. J. Khan, M. T. Iqbal, *Fuel Cells* **2005**, *5*, 463.

[14] J. C. Amphlett, R. M. Baumert, R. F. Mann, B. A. Peppley, P. R. Roberge, T. J. Harris, *J. Electrochem. Soc.* **1995**, *142*, 9.

[15] J. C. Amphlett, R. M. Baumert, R. F. Mann, B. A. Peppley, P. R. Roberge, T. J. Harris, *J. Electrochem. Soc.* **1995**, *142*, 1.

[16] R. F. Mann, J. C. Amphlett, M. A. I. Hooper, H. M. Jensen, B. A. Peppley, P. R. Roberge, *J. Power Sources* **2000**, *86*, 173.

[17] C. Bonnet, S. Didierjean, N. Guillet, S. Besse, T. Colinart, P. Carré, *J. Power Sources* **2008**, *182*, 441.

[18] B. A. Boukamp, *Solid State Ionics* **1986**, *20*, 31.

[19] M. Sluyters-Rehbach, J. H. Sluyters, *J. Electroanal. Chem.* **1970**, *26*, 237.

[20] R. F. Mann, J. C. Amphlett, B. A. Peppley, C. P. Thurgood, *J. Power Sources* **2006**, *161*, 768.

[21] Data provided by Hélion Fuel Cell Company.

[22] S. K. Mazumder, R. K. Burra, K. Acharya, *IEEE Transactions on Power Electronics* **2007**, *22*, 1437.

[23] *CRC handbook of chemistry and physics*, CRC Press, Boca Raton, FL, **2007**.

